CHAPTER 6

The study of Raman and transport properties in Fe doped $Bi_2(SeS)_3$

6.1 Introduction:

Insulators fascinates researchers to their complex electronic band structure and unusual electronic transport properties [152], [153]. TIs have many exotic properties like QAHE, giant linear magnetoresistance etc.[122]. Bi_2Te_3, Bi_2Se_3 and Sb_2Te_3[44]. TIs have been of great interest because of a single Dirac cone and enormous thermoelectric properties[154], [155]. TIs family contains some Bismuth and Antimony chalcogenides such as Bi_2Se_3, Bi_2Te_3 and Sb_2Te_3 3d-layered materials. One of the strong candidates of TI is Bi_2Se_3 which displays a quintuple layer structure ordered as Se-Bi-Se-Bi-Se sequence and has a topologically nontrivial band gap of 0.3ev[131], [156]. To achieve the best device application, it is essential to understand phonon dynamics in Bi_2Se3; especially phonon and electron-phonon interactions. To gain a good knowledge about electron-phonon and phonon dynamics, Raman scattering spectroscopy is a powerful and sensitive tool[157], [158]. It can reveal electronic structure, crystal structure, doping and lattice vibrations[156]. The vibrational properties of the material are associated with the carrier transport properties[159]–[161]. Bi_2Se_3 shows positive linear MR up to room temperature and displays SdH oscillations at low T and high magnetic field [131]. From SdH oscillations, one can extract the Π- Berry phase, which confirms the transport properties of 2D Dirac fermions[19], [162].

High-performance thermoelectric materials (TE) are needed for energy conversions, power generations, refrigerations and for solving future energy problems. TIs are good thermoelectric (TE) materials having a large thermoelectric power factor, which is very useful in energy conservation. The performance of TE materials is determined by the thermoelectric figure of merit, $ZT=S^2\sigma T$, where S is the Seebeck coefficient, σ is electrical conductivity T absolute temperature[154], [163].To enhance the ZT value, we need to increase the power factor value ($S^2\sigma$) and the low value of thermal conductivity. As we know,

Seebeck coefficient (S) and electrical conductivity (σ) are coupled with each other and inversely depends on carrier density. An appropriate value of carrier density can lead to a high value of thermopower. However, Bi_2Se_3 is known as an excellent thermoelectric material.

In the present study, we analyzed the role of electron-phonon in transport properties, the existence of the surface state and Dirac fermions as well as we studied the thermoelectric properties of $Bi_{2-x}Fe_xSe_{3-y}S_y$.

6.2 Experimental details

The single crystals of $Bi_{2-x}Fe_xSe_{3-y}S_y$ were synthesized by the modified Bridgemen method, which is reported elsewhere[60]. Obtained shiny silver single crystals could be easily cleaved along (00l) plane and characterized using a Rigaku (mini flex II DESKTOP) Powder diffractometer with Cu K_α radiation at room temperature, which is reported in our paper. Resistivity and magneto-transport measurements were carried by using a Quantum Design SQUID magnetic properties measurement system (MPMS). The thermoelectric measurement is performed with the homemade setup in our lab. A Temperature-dependent Raman study was done by Horiba LabRam HR evolution spectrometer. The sample was irradiated with the 633 nm output from a He-Ne laser kit (4.25 mW, 1800 groves/mm grating, slit width 400 nm) and Peltier cooled (-60 °C) CCD detector (model: Sincerity 356399, manufactured by Horiba Instrument Inc.) was used. For temperature-dependent Raman measurement, a software-controlled Micro-thermometric cell working in the temperature range of -193°C to 27°C (maker: Linkam) was used with 5 min equilibrium time. The spectra were recorded in the range 20 to 200 cm^{-1}.

6.3 Results and Discussions

Figure 6.1 shows a temperature-dependent resistivity curve at zero magnetic field. With increasing temperature, the value of resistivity is also increased, which indicates the metallic nature of $Bi_{2-x}Fe_xSe_{3-y}S_y$ down to 2K. At a higher temperature range (50K<T<300K), the variation of resistivity with the temperature is linear, suggesting the e-phonon scattering mechanism is dominating in the entire range. However, at the low-temperature range (2K<T<50K), the resistivity data can be fitted with the formula $R_{xx}=R_0+AT^m$ [A is a constant] with m=3.754 or 4. The value m=4 suggests a clear deviation from the pure electronic correlation dominated scattering mechanism (m=2). Such type of temperature-dependent resistivity is also seen in LaSb (m=4), LaBi (m=3) and Yttrium metals, as well as in other transition metals[164]–[166]. According to Ziman, s-d surfaces touch in a transition metal and the $\rho(T)\sim T^5$ and if the surfaces intersect each other, very complex nature of $\rho(T)$ is observed and $\rho(T)\sim T^4$. All the fitted values are lower than m=5, which is the pure e-phonon scattering phenomenon according to the Bloch-Gruneisen formula[165], [167]. From all the fitted values of n, we can conclude that at the lower temperature range, the interband s-d, e-phonon scattering mechanism dominates over s-s e-phonon scattering mechanism in $Bi_{2-x}Fe_xSe_{3-y}S_y$.

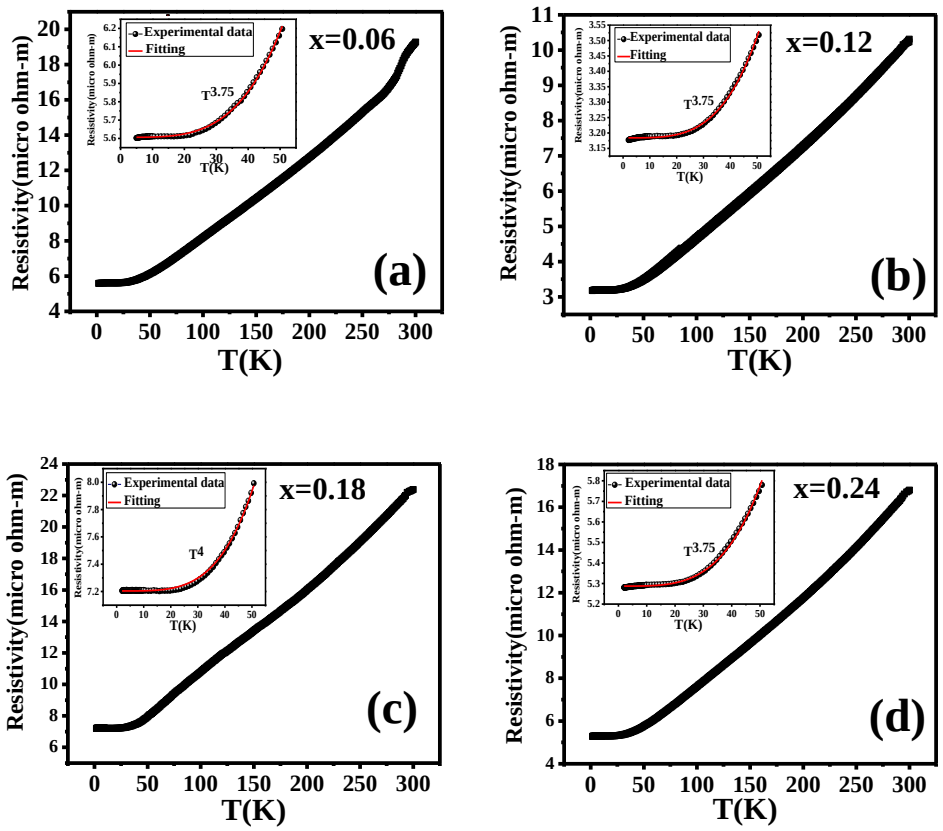

Figure 6.1: Temperature Variation of resistivity of $Bi_{2-x}Fe_xSe_{3-y}S_y$for **(a)** x=0.06, **(b)** x=0.12, **(c)** x=0.18, and **(d)** 0.24.

Figure 6.2 shows the variation of magnetoresistance with the applied magnetic field at different temperatures for $Bi_{2-x}Fe_xSe_{3-y}S_y$. Magnetoresistance can be expressed as MR% = (R(H)-R(0))/(R(0)) x100 where MR(H) is the resistance at the applied magnetic field (H), and MR(0) is the resistance at zero field. The direction of the magnetic field is perpendicular to the electric field. All the MR values are increased by increasing the magnetic field and decreased by increasing temperature. There is no sign of saturation up to 7T; unsaturated and linear behaviour of MR at high magnetic Field is advantageous in magnetic sensors [168]. But at low field, they show quadratic behaviour. According to the semiclassical model, the quadratic behaviour can be described as in the presence of the magnetic field, conduction electrons are deflected by the Lorentz force, and the square of the mobility is the prime factor

of this type of behaviour. The variation of MR with a high magnetic field is linear. In these materials, the non-saturating MR and high mobility are reported previously, and MR is proportional to carrier concentration[62], [63], [169]. The variation of MR with mobility is shown in figure 6.3. From figure 6.3, it is clear that MR is linearly varying with respect to mobility which is consistent with the theoretical and experimental results.[170]

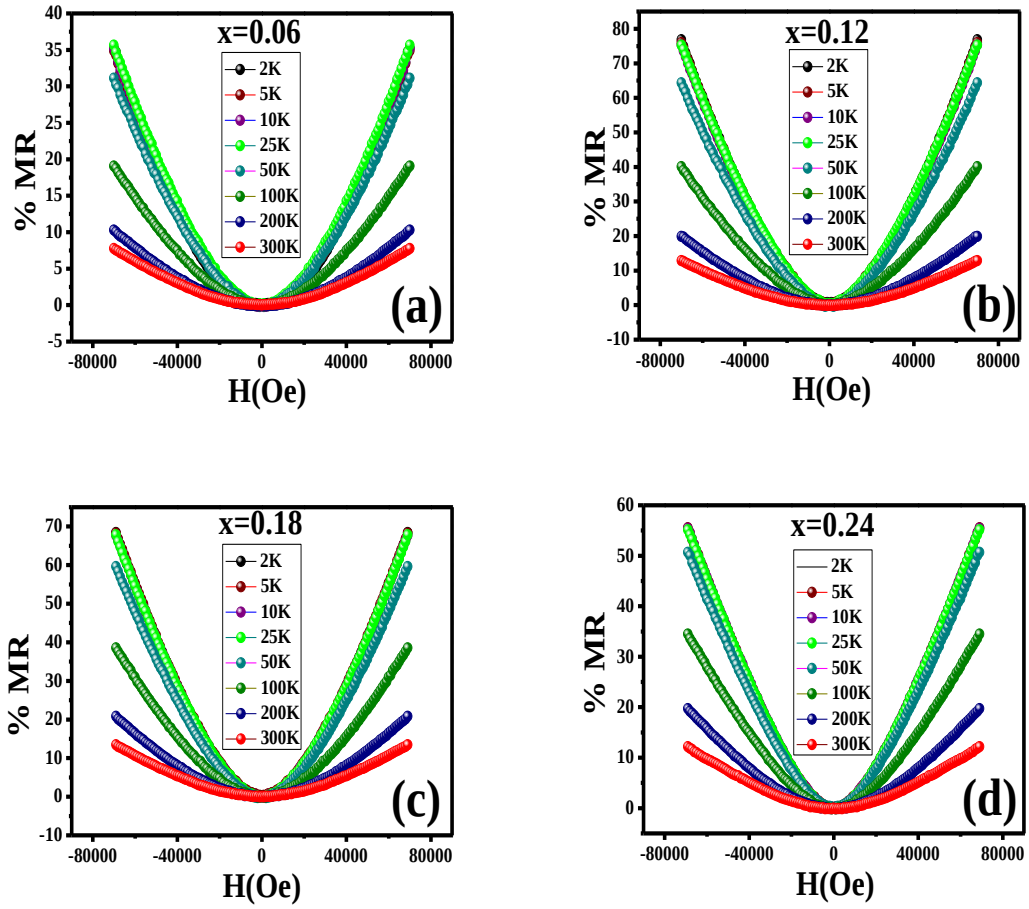

Figure 6.2: Magnetic field Variation of Magnetoresistance of $Bi_{2-x}Fe_xSe_{3-y}S_y$ for **(a)** x=0.06, **(b)** x=0.12, **(c)** x=0.18, and **(d)** 0.24 at different temperatures.

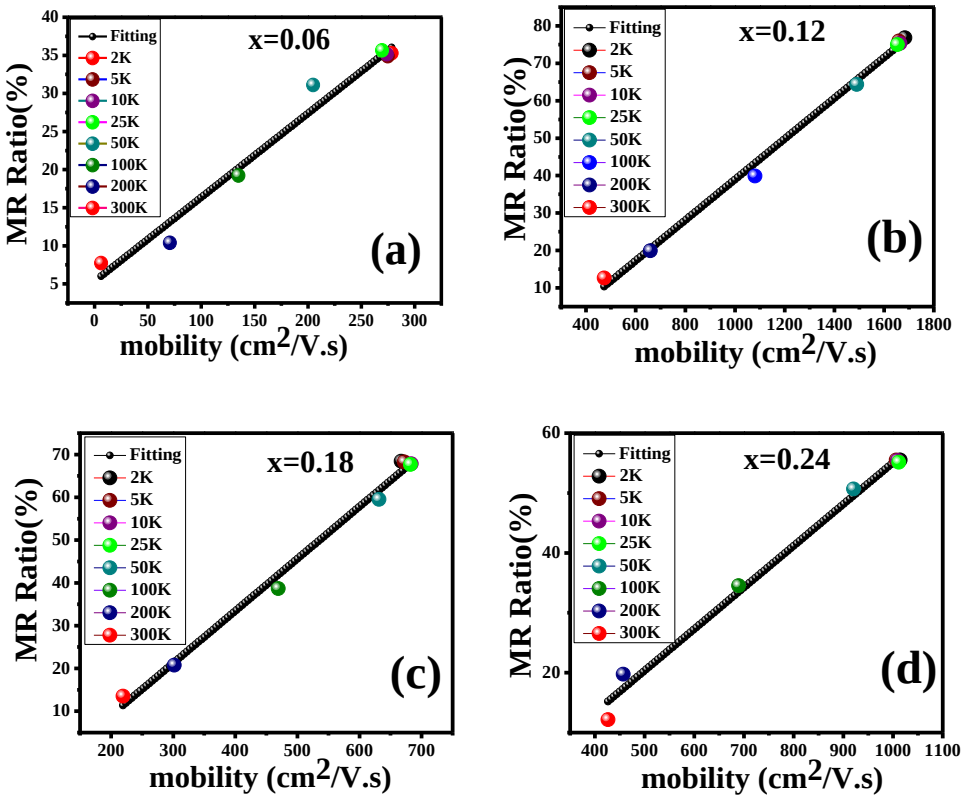

Figure 6.3: Magnetic field Variation of Magnetoresistance of $Bi_{2-x}Mn_xSe_{3-y}S_y$ for **(a)** x=0.12, **(b)** x=0.18. at different temperatures.

To further probe the surface state of a TIs, we have calculated the Landau level induced SdH oscillations. The Dirac states become quantized into landau levels when mag-field B is applied perpendicular to the surface state of the TI [171]. On increasing the magnetic field B, LLs lead to the SdH oscillations. In order to see the clear quantum oscillations, we have plotted $d^2\rho_{xx}/dB^2$ with respect to inverse applied field B^{-1}[170], which is shown in figure 6.4. For further confirmation of TSS, we determined the value of Berry phase β, which can be extracted from the Landau level fan diagram from the relation:

$$N=F/2\pi BN +\beta \quad (6.1)$$

Where, n represents the N^{th} Landau level. The maximum and minimum points have been taken as the full integer (N) and half integer (N+1/2) respectively. The graph between N and

$1/B_N$ gives a straight line and the slope of the line provides the Fermi surface cross-section [19], [101]. The value of β=0 and 0.5 enunciate about normal fermions and Dirac fermions, respectively. If β is near about 1/2 leads to the π Berry phase and suggests that the oscillations originate from the surface helical state [55], [171]. The slope of the Landau level Fan diagram gives us the value of oscillating frequency, F. A_f is the Fermi surface cross-section which can be determined by using Onsager's relation, $F= \hbar A_f/2\pi e$. From the circular assumption, $A_f = \pi K_f^2$ and $A_f = (2\pi)^2 n_s$, we have calculated the value of Fermi wave vector K_f and surface carrier concentration n_s, if we consider that the K_f corresponds to 2-D Fermi surface. The bulk carrier concentration is also determined if we assume that the K_f corresponds to 3-D Fermi surface. All the determined values of all the samples are mentioned in table 6.1. The obtained value K_f in order of 10^6/cm, which is slightly less than the reported values [110], [172], indicating the closer proximity of the Fermi level to the Dirac point [110]. For $Bi_{2-x}Fe_xSe_{3-y}S_y$ (x=0.06 and x=0.12), the obtained value of β is 0.56 and 0.59, respectively, which is close to 0.5, suggesting the existence of the surface state and for x=0.18 and x=0.24, the value of β is far away from 0.5 confirming the surface state deteriorates on increasing the doping concentration of Fe and S. These results are consistent with the other reports [110], [171], [172]. Therefore, from all these calculations, we conclude that on increasing doping surface state becomes weaker gradually.

Table 6.1. All the obtained parameters from Hall and LL calculations.

Composition $Bi_{2-x}Fe_xSe_{3-y}S_y$	**Fermi wave vector (K_f) (2K)**	**Surface carrier concentration (n_s) (2K)**	**Bulk carrier concentration (n_b) (2K)**		**Mobility (μ) (2K)**
			Hall Calculation	**LL Calculation**	
x=0.06	4.91× 10^6 /cm	1.92×10^{12} /cm^2	1.20×10^{19} /cm^3	4.011×10^{18} /cm^3	3262 cm^2/V.S
x=0.12	4.92× 10^6 /cm	1.93×10^{12} /cm^2	1.06×10^{19} /cm^3	4.03×10^{18} /cm^3	2049 cm^2/V.S
x=0.18	4.54× 10^6 /cm	1.64×10^{12} /cm^2	9.86×10^{18} /cm^3	3.16×10^{18} /cm^3	879 cm^2/V.S
x=0.24	5.85× 10^6 /cm	2.72×10^{12} /cm^2	7.02×10^{18} /cm^3	6.76×10^{18} /cm^3	1685 cm^2/V.S
$Bi_{2-x}Mn_xSe_{3-y}S_y$ **x=0.12**	5.86× 10^6 /cm	2.74×10^{12} /cm^2	1.16×10^{19} /cm^3	6.82×10^{18} /cm^3	1024 cm^2/V.S
x=0.18	4.16× 10^6 /cm	1.38×10^{12}/cm^2	1.96×10^{19} /cm^3	2.43×10^{18} /cm^3	1770 cm^2/V.S

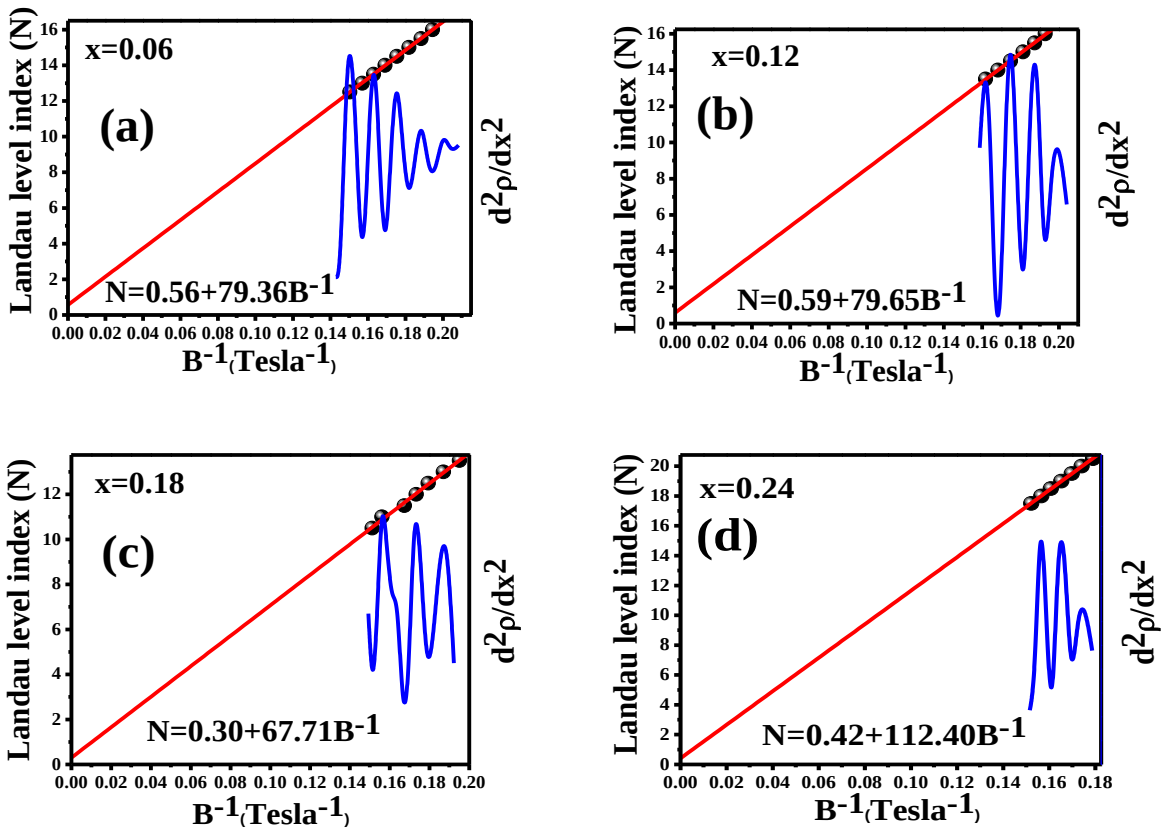

Figure 6.4: Landau Level Fan diagram of $Bi_{2-x}Fe_xSe_{3-y}S_y$ (a) x=0.06, (b) x=0.12, (c) x=0.18, and (d) 0.24.

In metals, the variation of magnetoresistance with the temperature and magnetic field illustrated by Kohler's rule. According to semiclassical theory, Kohler's rule stabilized when a single type of charge carrier existed and the same scattering rate at all the points of the Fermi surface[173]. Kohler's rule can be written as;

$$MR=(B/\rho_{xx}(0))^{\alpha} \quad (6.2)$$

Where $\rho_{xx}(0)$ is the resistance at zero field and α is a constant. All the MR curves at different temperatures and fields should merge into a single curve. Figure 6.5 shows all the curves are scaled on the same curve and in good agreement with Kohler's plotting. There is a little deviation at 300K that might be due to electron-phonon scattering. We have fitted the

data at low temperature and find out the value of α, as 1.61<α<1.87, which is very close to 2 [inset of figure 6.5], suggesting that it is a perfectly compensated system [174].

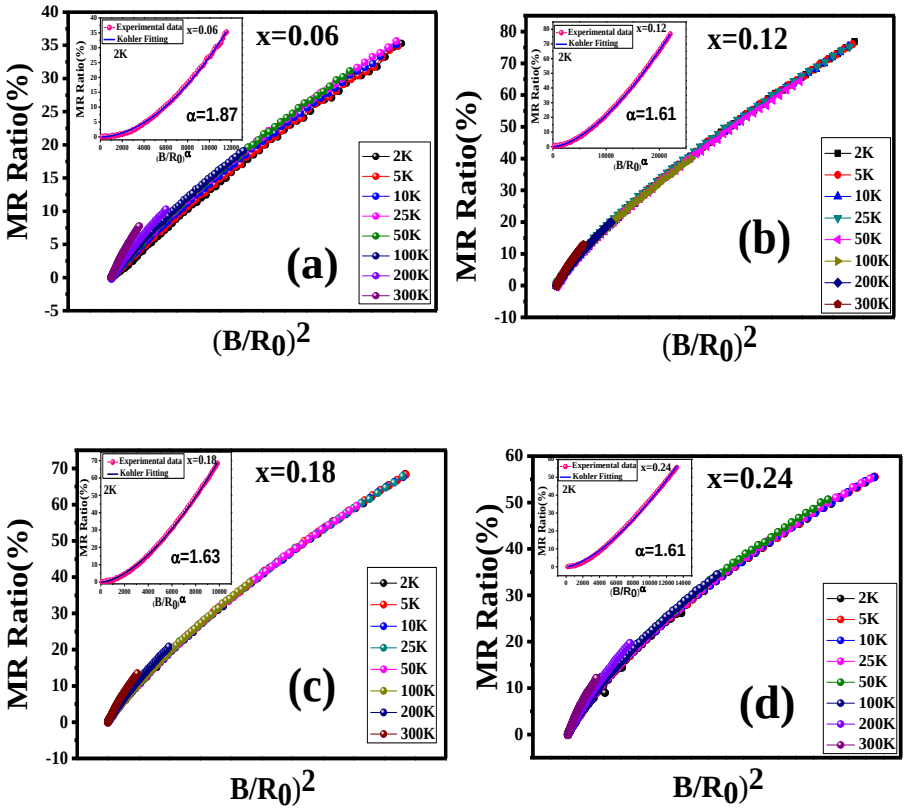

Figure 6.5: Kohler scaling of $Bi_{2-x}Fe_xSe_{3-y}S_y$. **(a)** x=0.06, **(b)** x=0.12, **(c)** x=0.18, and **(d)** 0.24.

To shed more light on the transport properties, we have performed thermoelectric measurement of the sample. We have calculated Seebeck coefficient S and power factor, $PF=\sigma S^2$ of our sample where σ is the electrical conductivity and S is the Seebeck coefficient[175]. The temperature (T) vs. thermopower (S) curve is shown in figure 6.6 (b) (c) (d) and (e) in the temperature range 25K-300K. The negative value of the Seebeck coefficient reveals that our sample has n-type conductivity, which is consistent with the Hall data[122] and other reports[163], [176]. The electrical resistivity increases with increasing

temperature, and the value of thermopower is also increasing with increasing temperature. Thermopower in the degenerate doping limit is given by;

$$S=\frac{K}{e}\left(\frac{\pi^2 KT}{3E_f}\right)\left(\frac{3}{2}+r\right) \quad (6.3)$$

E_f is the Fermi energy, and r is the index of relaxation time that belongs to kinetic energy[177]. The first term of Eq^n presents the conventional inverse coupling between S and σ, and the second term allows the decoupling of them. The value of r =-1/2 for acoustic phonon scattering and 3/2 for ionized impurity scattering. In the present study, the nature of the measured Seebeck coefficient curve follows the trend for (r=-1/2), which supports the fact that electrons are scattered by phonons. The value of carrier concentration ~($\times 10^{19} cm^3$)[122] in the samples is limited by phonon scattering[177], [178].

The calculated value of the Seebeck coefficient is -103.74 micro-volt/K at 300K, which is quite good, and the power factor has the highest value 657.71 microwatt-K^{-2}.m at 236Kwhich is shown in figure 6.6. From here, it is clear that it has a very large power factor at 236K and 300K. Therefore, it is important for potential applications at room temperature. Single crystals have very high thermal conductivities. Due to this, they have a large power factor at low temperature as compared to room temperature [9]. Still, our sample shows a large power factor at room temperature, and it is quite good for room temperature potential applications.

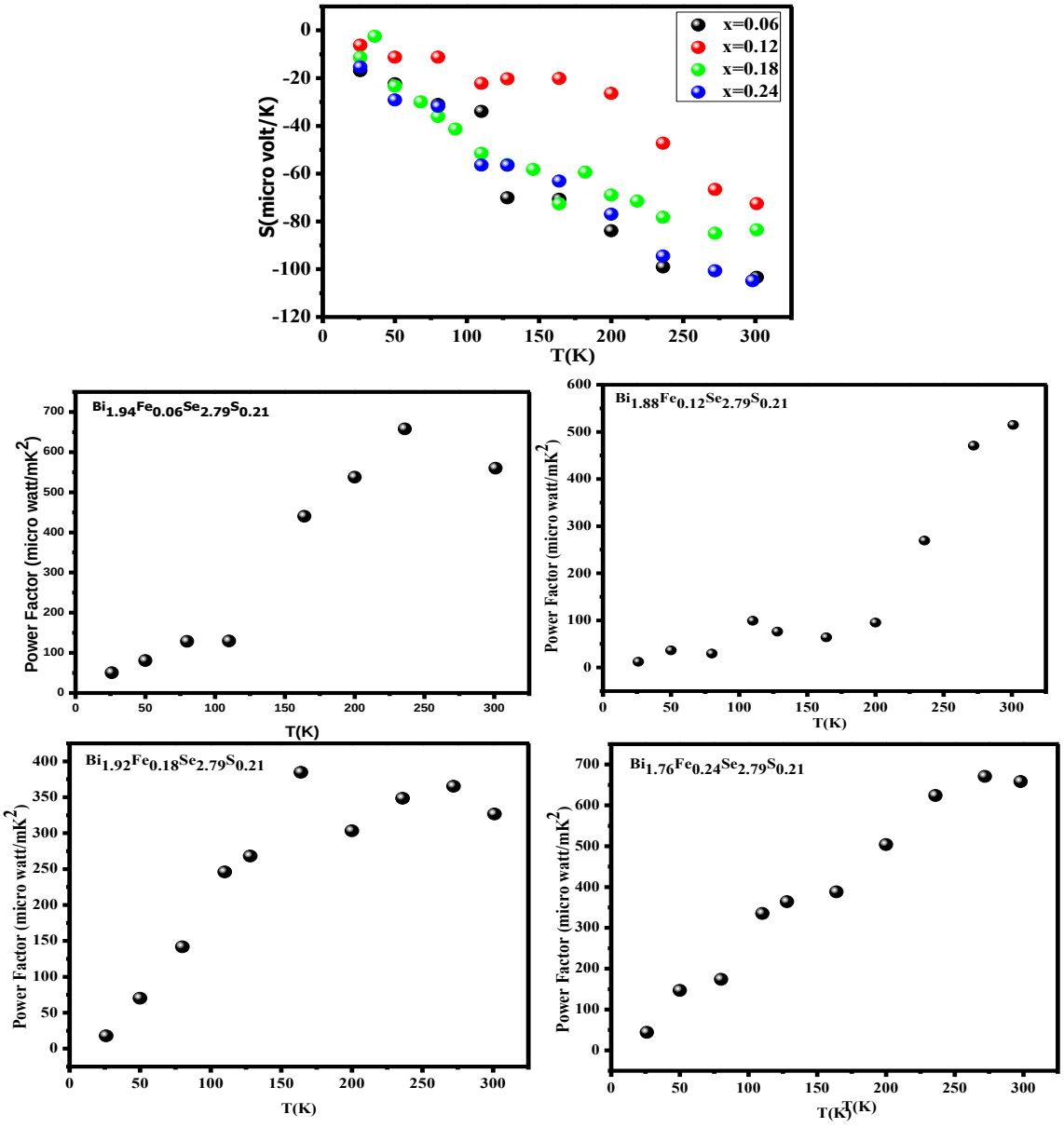

Figure 6.6: (a) Measured value of Seebeck coefficient for all the samples and calculated value of power factor with respect to temperature (b**)** x=0.06, (c) x=0.12, (d) x=0.18, and (e) 0.24.

6.3.1 Raman Study:

The crystal structure of Bi_2Se_3 is rhombohedral and have D^5_{3d}(R3-m) space group symmetry. The atomic arrangement of Bi_2Se_3 is unique. It consists of a sandwich structure of repeating units that display quintuple layer structure ordered as Se-Bi-Se-Bi-Se sequence, weakly bounded by Wanderwall forces. With 5 atoms per unit cell, there are 15 lattice dynamical modes, three acoustic and 12 optical phonon modes. Out of 12 optical phonons, 4 are Infra-Red (IR) active such as $2A_{2u}+2E_u$, and 4 are Raman active $2A_{1g}+2E_{1g}$ with the frequencies in the 30 to 200cm^{-1} range[33]. The irreducible representations for the zone center phonons can be written as;

$$\Gamma = 2E_g+2A_{1g}+2E_u+2A_{1u} \tag{6.4}$$

The Raman tensors of Bi_2Se_3 can be expressed as;

$$A_g=\begin{pmatrix} a & 0 & 0 \\ 0 & a & 0 \\ 0 & 0 & a \end{pmatrix},\quad E_g=\begin{pmatrix} c & 0 & 0 \\ 0 & -c & d \\ d & 0 & 0 \end{pmatrix},\begin{pmatrix} 0 & -c & d \\ -c & 0 & 0 \\ d & 0 & 0 \end{pmatrix}$$

One can easily differentiate E_g and A_{1g} modes from one to another. The A_g has a vanishing component off diagonally, but E_g mode has nonvanishing off-diagonal elements[179].

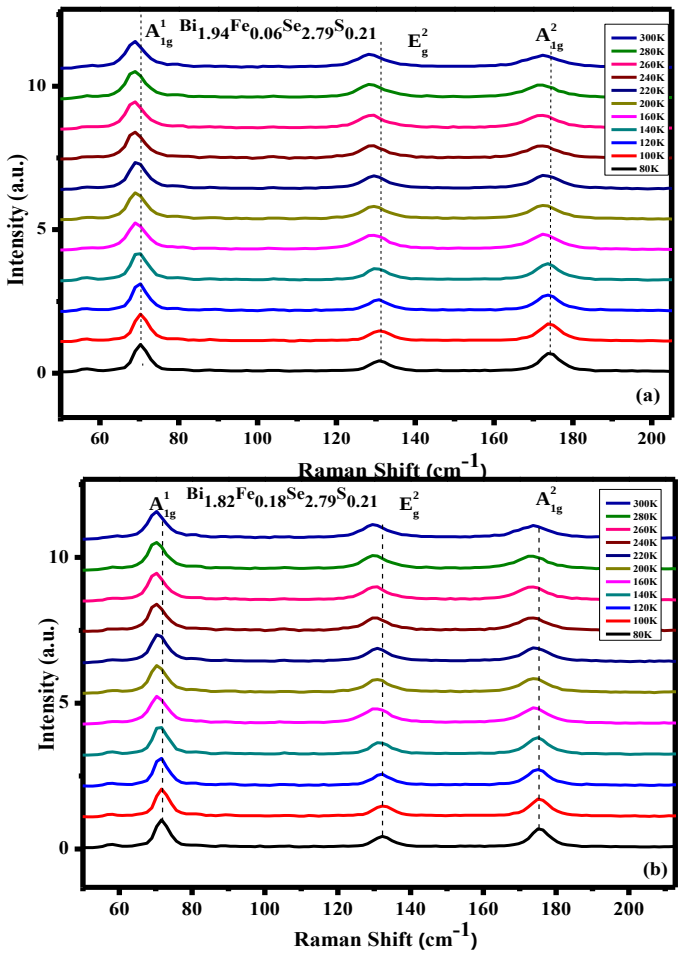

Figure 6.7: Temperature dependent Raman Spectra for **(a)** x=0.06, **(b)** x=0.18.

To understand phonon behaviour, the study of temperature-dependent vibrational modes is very useful. We carried out the systematic temperature-dependent. For the detailed and systematic temperature-dependent Raman study, we collected the Raman spectra of Bi_2Se_3 in the temperature range 80K to 300K as we can see in figure 6.7 that the intensities of all the Raman active modes are good to study the effect of temperature on FWHM and peak positions. On decrement in temperature, the increment in intensities of Raman spectra was observed significantly to follow the red shift. The FWHM increases on increasing

temperature; we have fitted the spectra with the Lorentzian fit and extracted peak positions and FWHM, which is shown in figure 6.8(a) and (b)).

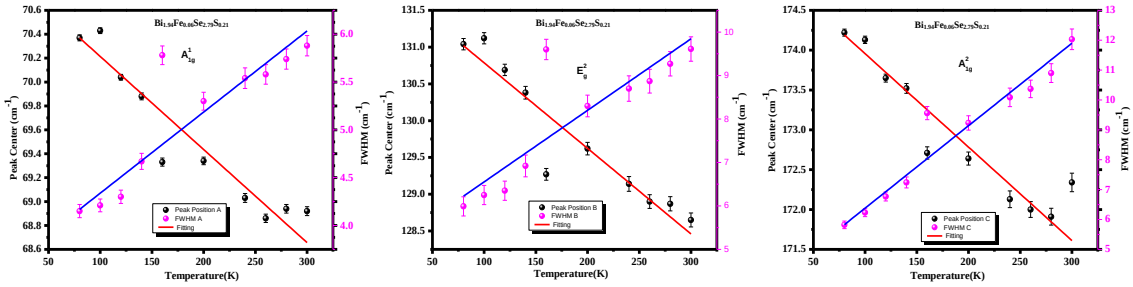

(a)

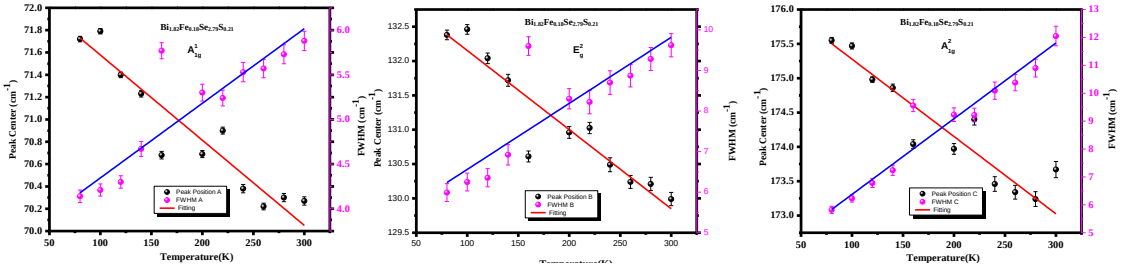

(b)

Figure 6.8: Variation of Peak positions and FWHM with the Raman shift **(a)** x=0.06, **(b)** x=0.18.

For pure Bi_2Se_3 single crystal, the Raman active A_{1g}^1cm^{-1}, E_g^2cm^{-1}and A_{1g}^2cm^{-1} modes have been observed at 72cm^{-1},131cm^{-1},175cm^{-1}. The frequency of A_{1g}^1 mode shifted from 72cm^{-1} to 68cm^{-1}, E_g^2 mode shifted from 131cm^{-1} to 128cm^{-1} and A_{1g}^2 mode shifted from 174cm^{-1} to 172cm^{-1}. To probe the thermal expansion, thermal conductivity and interlayer coupling, the temperature-dependent Raman is very helpful. All the Raman peaks clearly show redshift on increasing temperature from 80K to 300K. In figure 6.8, it can be clearly seen that peak positions have a linear dependency on temperature. Due to thermal expansion and contraction of the crystal and phonon mode leads to anharmonicity, and the temperature-dependent Raman spectroscopy may arise due to anharmonicity[180]. The temperature-dependent

intensity and width could be attributed to the zone-center optical phonon decaying into an optical phonon and acoustic phonon[181]. We have fitted the spectra by a linear equation which can be written as;

$$\omega(T)=\omega_0+\chi T \quad (6.5)$$

Where ω_0 is the vibrational frequency at zero temperature, χ is the first-order temperature coefficient of E_g^2 or A_{1g}^2 modes. The obtained values of the first-order temperature coefficient. χ for each Raman mode listed in table 6.2. The low value of χ(temperature coefficient) is the foremost to get a high power factor value[159], [181]. The value of the power factor for Fe is quite high, which is 657.71 microwatt-K^{-2}. Thus, we can say our Raman study and thermoelectric study is well connected as well as transport measurement also confirms the significant role of phonons in the materials.

Table 6.2. The value of First order temperature coefficient of each Raman mode for $Bi_{1.94}Fe_{0.06}Se_{2.79}S_{0.21}$ and $Bi_{1.82}Fe_{0.18}Se_{2.79}S_{0.21}$.

Sample name	Raman mode	χ- value
$Bi_{1.94}Fe_{0.06}Se_{2.79}S_{0.21}$	A_{1g}^1	-0.72×10^{-2}
	E_g^2	-1.16×10^{-2}
	A_{1g}^2	-1.17×10^{-2}
$Bi_{1.82}Fe_{0.18}Se_{2.79}S_{0.21}$	A_{1g}^1	-0.76×10^{-2}
	E_g^2	-1.15×10^{-2}
	A_{1g}^2	-1.12×10^{-2}

6.5 Conclusion

At the lower temperature range, the interband s-d e-phonon scattering mechanism dominates over s-s e-phonon scattering mechanism in $Bi_{2-x}Fe_xSe_{3-y}S_y$. The value of $\beta=0$ and 0.5 enunciate about normal fermions and Dirac fermions, respectively. If β is near about 1/2 leads to the π Berry phase and suggests that the oscillations originate from the surface helical state. The value of α, is very close to 2 [inset of figure 6.5], suggesting that it is a perfectly compensated system. It has a very large power factor at 236K and 300K. Therefore, we can

use it at room temperature. The low value of χ (temperature coefficient) is the foremost to get a high power factor value.